PAPER

Performance recovery of plasma actuators in wet conditions

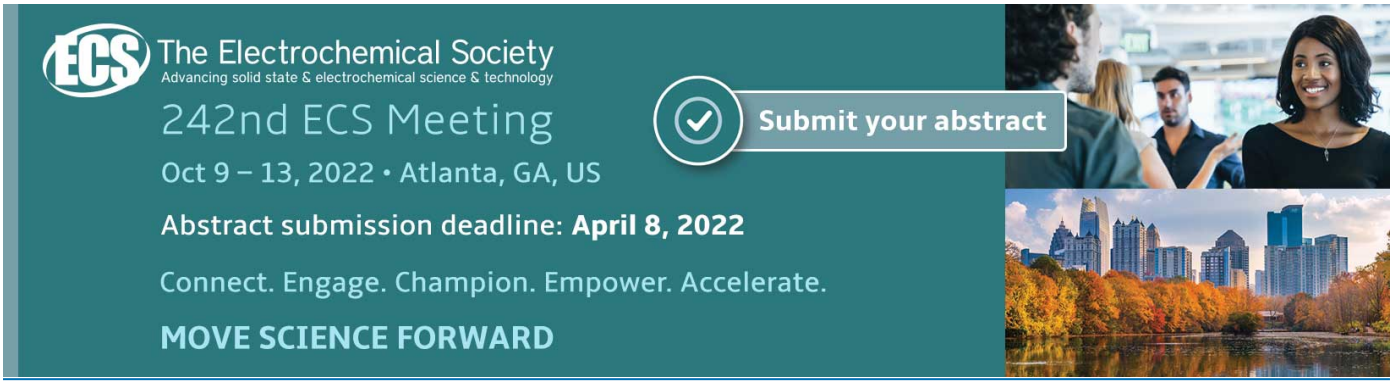

IOP Publishing Journal of Physics D: Applied Physics
J. Phys. D: Appl. Phys. **55** (2022) 155201 (14pp) https://doi.org/10.1088/1361-6463/ac472d

Performance recovery of plasma actuators in wet conditions

Alexander James Lilley, Sarthak Roy, Lucas Michels and Subrata Roy*

Applied Physics Research Group, University of Florida, Gainesville, FL, 32611, United States of America

E-mail: roy@ufl.edu

Received 6 September 2021, revised 21 December 2021
Accepted for publication 30 December 2021
Published 19 January 2022

Abstract

Plasma actuators have been extensively studied for flow control applications over the past two and a half decades. While these studies have been traditionally focused on characterizing their performances as flow control devices, the performance of plasma actuators under adverse conditions such as dew or light rain remains to be less explored. This paper seeks to study the effects of water adhesion from droplets directly sprayed on to a plasma actuator using thrust recovery as the performance metric. It was found in all tests that wet actuators quickly recover plasma glow, before gradually regaining performance comparable to the dry actuator. The measured thrust for the wet actuator after 5 s of operation recovered by 46% and 42% of the thrust of the dry actuator for 50.0–62.5 g m^{-2} and 125–150 g m^{-2} of sprayed water droplets, respectively. At 22.5 kV_{pp} and 14 kHz, the highest thrust recovery was recorded at 84% of that of the dry actuator after 80 s of operation. For 17.5 kV_{pp} and 14 kHz the wet thrust recovered by 79%, while for 22.5 kV_{pp} and 10 kHz the wet thrust recovered by 68% of their dry counterpart in 80 s. For 17.5 kV_{pp} and 14 kHz, the thrust almost fully recovered in comparison to the dry actuator after about 290 s of operation. These results indicate that both applied voltage and operating frequency plays a critical role in the performance recovery while the latter may have a stronger influence. Performance recovery for a wet serpentine shaped plasma actuator is also included for general applicability. The power data in all cases show that wet actuators consume more power which with time gradually approach the dry actuator power data. This is because during the initial stages of operation, the rolling mean current of the wet actuator is higher than the dry actuator even though the ionization spikes of dry actuator is stronger.

Keywords: performance, recovery, plasma, plasma actuator, dielectric barrier discharge, rain, wet and dry

(Some figures may appear in colour only in the online journal)

1. Introduction

Plasma actuators have been extensively studied for flow control applications since the 1950s [1]. There is a wide variety of plasma actuators that operate in the regime of high (>1000 K) to low (<400 K) temperature plasmas requiring high kilowatts to low watts of power. While the arc jets are in the former regime, the glow discharge plasmas are in the latter. Specifically, dielectric barrier discharge (DBD) plasma actuators are of this latter class that use at least an embedded electrode and an exposed electrode separated by at least an insulating material. A high (kV) voltage, low amplitude (mA) alternating current is applied between these two asymmetrically positioned electrodes at a high (kHz) frequency, and through an ionization process transfers Lorentzian momentum to the neighboring fluid by which charged particles weakly collide with neutral particles [2–4]. DBD plasma actuators are extremely attractive as flow control devices due to their surface compliance, light weight, high-frequency response, and lack of moving parts. DBD plasma actuators have proposed usage in pitch

* Author to whom any correspondence should be addressed.

control, roll control, separation control, and flaps [5–7]. Many studies have shown the potential use of plasma actuators as flow control devices across a wide range of flow applications. Examples include control of transition to turbulence [8–10], drag reduction for highway vehicles [11–13], lift to drag ratio modification for flow over a wing [14, 15], flow modification over bluff bodies [13, 16], blade vortex interaction noise control [17], flight control for small aircrafts and projectiles [18, 19] and deicing application [20–22]. However, environmental ruggedness and performance reliability of these actuators must be studied before their practical implementation for any external flow applications.

Studies have shown the environmental impact on plasma actuator performance [23–25]. Benard *et al* [24] measured the ionic wind velocity induced by a plasma actuator operating at 32 kilovolts peak to peak (kV_{pp}) and 1 kHz frequency as a function of ambient pressure. As pressure went down the induced airflow kept increasing from 2.5 m s^{-1} at 101 kPa till it reached a maximum of 3.5 m s^{-1} at 60.6 kPa and then it gradually dropped down to 3 m s^{-1} at 20.2 kPa. Soni and Roy [25] reported that as the ambient pressure decreases from 101 to 13 kPa plasma induced thrust increases to a maximum as a function of applied electric field, then drops steadily approaching zero while the power consumption monotonically increases. Based on experiments performed, a set of correlation functions was established between the maximum induced thrust, ambient pressure and nominal applied electric field. The effect of dielectric material on thrust and ozone production has also been extensively studied as a function of effective (normalized by relative dielectric constant) thickness by Wilkinson *et al* [26] and Portugal *et al* [27].

Plasma actuators for external flow control applications are limited by wet operating conditions. While a moderate increase in humidity has been shown to increase the performance of DBD actuators [28, 29], high relative humidity (RH) with dew point approaching the ambient temperature is generally recognized as detrimental to the efficacy of DBD actuators [30–32]. The functional metric of the actuator (for example, induced thrust) must be quantified as RH approaches 100%. Specifically, identifying the behavior of the body force inducement as a function of RH would be quite useful for determining the operational envelope of the DBD actuator for external flow applications like that on automobiles, trucks, and aircrafts. Previous efforts reported include initial experiments by Anderson and Roy [28] assessing the effect of RH on the surface pressure coefficient. They showed a modest increase in actuator performance with RH for narrow range of $43\% \leqslant \mathrm{RH} \leqslant 53\%$. Benard *et al* [29] reported performance of a DBD plasma actuator for a wider range of $40\% \leqslant \mathrm{RH} \leqslant 98\%$ using a sinusoidal AC voltage with amplitudes ranging from 16 to 24 kV at 1 kHz, highlighting that while DBD actuators could operate at high RH, the induced air velocity reduced with increased RH. Interestingly, as RH increased, the number of positive and negative current peaks decreased. Wicks and Thomas [30] documented that the reactive thrust of the actuator significantly reduced for higher levels of RH approaching 70%. They approximated the thrust reduction as a power-law relation with ambient RH. The power-law exponent increased with applied voltage but decreased by a factor of $\sqrt{2}$ beyond a threshold RH of 70%.

The operability in environments that can be considered as challenging for actuator performance is of great interest in the maturation of the system. Clearly more focused research is needed in this area, especially addressing the environmental concerns of the effect of direct water deposition on the thrust performance of the plasma actuator. This is crucial because in practical implementations, actuators are likely to be exposed to saturated humidity conditions due to rain, fog or in different categories of clouds during a flight. Therefore, from an engineering perspective, there is a fundamental need to study the actuator performance for wet conditions.

This paper aims to explore the effect of a collection of water droplets on thrust and power as a function of operating voltage, frequency, and water adhesion on a plasma actuator. To our knowledge, no such work has been reported in published literature. The lack of published work in peer-reviewed journals is undoubtedly related to the many difficulties of this type of study. One major difficulty is reproducibility of the deposition of droplets whose size distribution may vary greatly. The presence of an external flow constitutes an additional technical challenge requiring the implementation of complex testing equipment. This paper focusses on comparing the thrust performance of DBD plasma actuator for two specific sinusoidal input voltages and frequencies under dry and wet conditions without any external flow. The size distribution of deposited water droplets is also quantified for future experiment reproducibility.

2. Experimental setup and procedure

All experiments were performed within the Applied Physics Research Group quiescent chamber. The chamber measures 0.61 × 0.61 × 1.22 m. The general setup for thrust measurement is shown in figure 1. This is the same setup as Durscher and Roy [32]. The setup consists of an acrylic stand, an O'Haus scale, Faraday's cage, amplifiers, oscilloscope, and function generator in a quiescent chamber. Specific information is given in each subsequent section.

2.1. Actuator design

To make the results of this experiment applicable to the most variants of SDBD actuators, a standard linear actuator shape was used for measuring the power and induced thrust. It is assumed that the results can then be extrapolated to other actuator shapes like sawtooth, sinusoidal, and square waves. As a performance demonstration of a generic actuator geometry under wet conditions, the glow (performance) recovery of a set of square wave actuators was also demonstrated.

The linear actuator schematic is shown in figure 2. The dimensions for the exposed electrode a, the embedded electrode c, the actuator plate length L and width W are given alongside in a tabulated form. The embedded electrode is placed 1.0 mm (b) horizontally downstream of the exposed electrode. These electrodes are vertically separated by a 3 mm

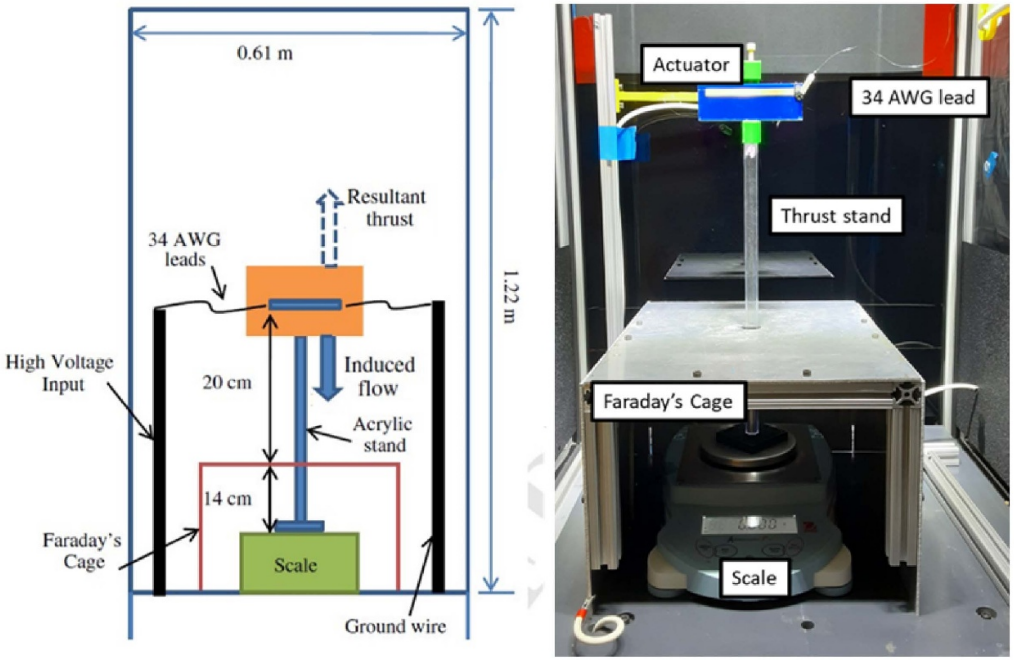

Figure 1. Depiction of the experimental setup, taken from Durscher and Roy [32]. On the right, a photo of the actual setup with relevant components labeled.

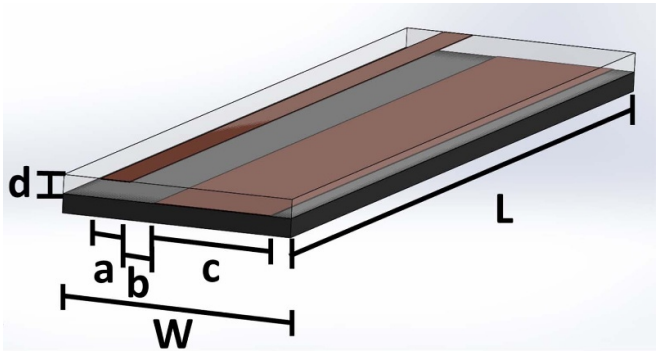

Dimensions in mm

a	*b*	*c*	*d*	*L*	*W*
6.35	1.0	25.4	3.0	100.0	40.0

Figure 2. Schematic of the linear actuator.

(*d*) thick acrylic with a relative dielectric constant of 3.2. The ratio of the length of the exposed and embedded electrode (*a:c*) is 1:4 [32]. The surface tension and contact angle for the acrylic material are 37.5 mJ m^{-2} and 70.9°, respectively [33]. This information is solely included for completeness since wettability is not being studied in the present work.

For the set of square wave serpentine actuators, the dielectric material is RO4350B which has a relative dielectric constant of 3.66 and a dielectric strength of 312 kV cm^{-1}. While no wettability information for this material can be found, the material is known to have a 0.06% moisture content reported for 48 h immersion of 1.52 mm sample at 50 °C [34]. Figure 3 shows dimensional details of the tested actuator. The thickness of the actuator plate is 0.88 mm. Since the thrust generated by this actuator is strongly 3D ([9], see figures 1 and 2), only power data will be presented for this case to show the influence of water spray on its performance.

2.2. Ohaus adventurer pro scale

The Ohaus Adventurer Pro Scale used for the thrust measurement has a sampling rate of 1 Hz and ±0.001 g accuracy. A 3.18 mm thick aluminum Faraday cage is used to prevent electromagnetic interference with the scale [32]. This thickness was chosen simply due to the availability and ease of machinability. An acrylic base is used to mate the scale to the actuator as seen in figure 1. A 3D-printed clamp with a glass reinforced nylon screw is used to clamp the actuator in place such that the induced thrust is upwards (see figure 1).

2.3. Electrical setup

To power the plasma actuator the following arrangement is used as shown in figure 4. A Tektronix AFG3022B arbitrary function generator is used to create the sinusoidal signal, which is fed into a QSC RMX 2450 audio amplifier. The QSC

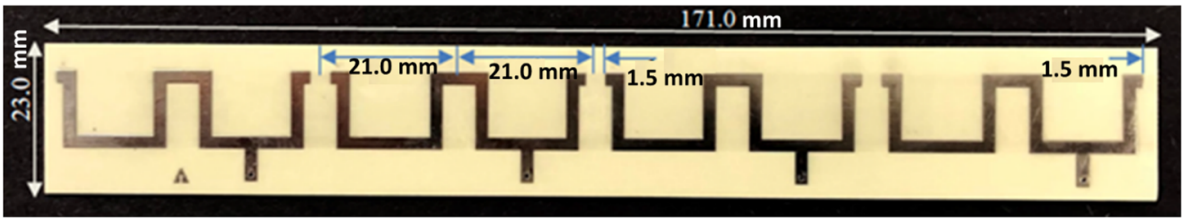

Figure 3. Geometric dimensions in mm of the square wave serpentine actuator.

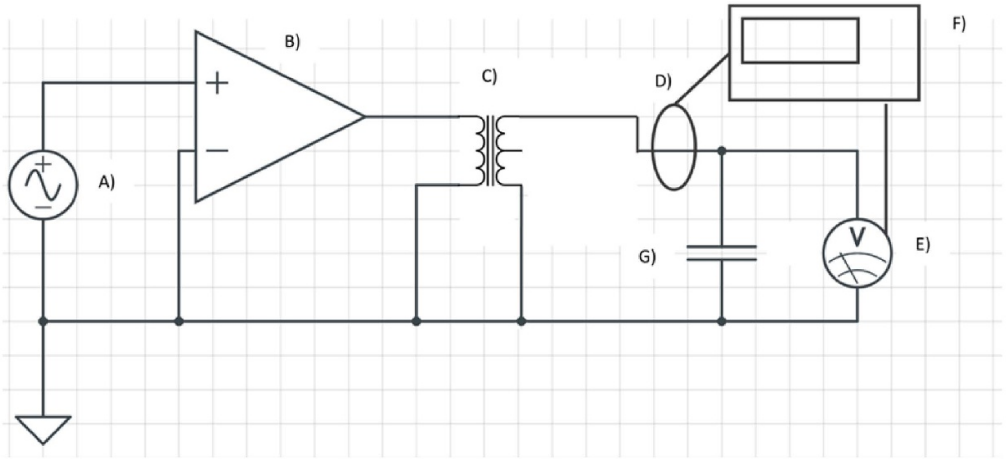

Figure 4. The electronic setup for powering the actuator. (A) Tektronix AFG3022B arbitrary function generator. (B) QSC RMX 2450 audio amplifier. (C) Corona magnetics custom transformer. (D) Pearson electronic 2100 current probe. (E) Tektronix P6015a. (F) Tektronix DPO3014 oscilloscope. (G) Linear plasma actuator.

amplifier output is sent to a custom-made Corona Magnetics transformer with a transformer ratio of 1:245 and a frequency response of 8–30 kHz. A Tektronix P6015a voltage probe is used to measure the voltage. The sinusoidal output from the voltage probe is measured using a Tektronix DPO3014 Oscilloscope (see figure 5). The current is measured using a Pearson Electronic 2100 current probe. The current probe's output is sent to the oscilloscope. The plasma actuator has the embedded electrode grounded and the exposed electrode connected to the Corona Magnetics transformer output. The voltages explored are on the order of 10 kilovolts peak to peak (kV_{pp}).

2.4. Thrust measurement procedure

Table 1 describes seven separate cases experimentally investigated for thrust study using the actuator shown in figure 2. In case 1, the dry actuator is run at 22.5 kV_{pp} and 14 kHz, which serves as the baseline case. In case 2, the actuator is wet with 0.20–0.25 g of water and is run at 22.5 kV_{pp} and 14 kHz. In case 3, the actuator is wet with 0.50–0.60 g of water and is run at 22.5 kV_{pp} and 14 kHz. Note that when divided by the total area of the actuator plate the ensemble average water content becomes 50.0–62.5 g m^{-2} and 125.0–150 g m^{-2}, respectively. The latter amount of water seems, visually, to be the point of saturation beyond which the water starts to run off the actuator making the scale reading unstable. In case 4, the dry actuator is run at a 17.5 kV_{pp} and 14 kHz. In case 5, the actuator is wet with 0.20–0.25 g of water and run at 17.5 kV_{pp} and 14 kHz and results are compared with case 4. In case 6, the dry actuator is run at 22.5 kV_{pp} and 10 kHz. In case 7, the actuator is wet with 0.20–0.25 g of water and is run at 22.5 kV_{pp} and 10 kHz and results are compared with case 6. For all cases the scale measures the weight at a sampling rate of 1 Hz. All cases were run at an ambient temperature of 21 °C and a RH of 70%. Tap water with a resistivity of 40 $\Omega \cdot m$ was used for all wet experiments [35].

Water is sprayed from a fixed location, at a normal distance of 20 cm, directly away from the center of the actuator. This process is repeated until the weight of the water is within the desired range. Approximately 25 s of settling period is then allowed prior to turning on the actuator to visually ascertain that the water adhesion is steady, i.e. there is no dripping of water droplets from the plate.

2.5. Approximation of water evaporation on a running a plasma actuator

For wet cases (2, 3, 5, 7, and 9), it is difficult to separate the weight of the water on the actuator that is continuously evaporating from the thrust generated by the actuator. For the dry actuator case the thrust can be measured directly [32]. For the cases 2, 3, 5, 7, and 9, where water is added to the actuator, the evaporation of water is approximated using a function. The initial weight of water added prior to turning on the actuator is

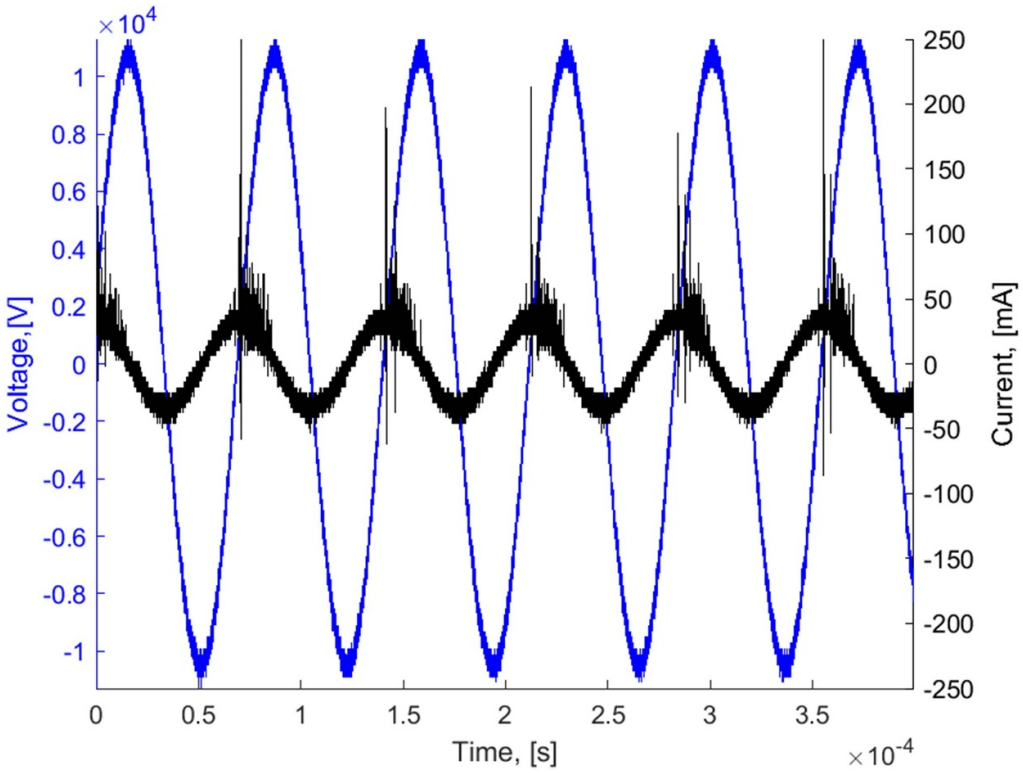

Figure 5. The representative waveforms case 1, 22.5 kV_{pp} 14 kHz. The voltage plotted in blue is a sinusoidal waveform with axis labelled on the left. The current is plotted in black with axis labeled on the right.

Table 1. Cases considered.

Cases	Voltage (V)	Frequency (Hz)	Condition (g of H_2O)	g m^{-2} of H_2O	Experiment duration (s)
1	22 500	14 000	0.00 (dry)	—	80
2	22 500	14 000	0.20–0.25	50.0–62.5	80
3	22 500	14 000	0.50–0.60	125.0–150.0	80
4	17 500	14 000	0.00 (dry)	—	80
5	17 500	14 000	0.20–0.25	50.0–62.5	80
6	22 500	10 000	0.00 (dry)	—	80
7	22 500	10 000	0.20–0.25	50.0–62.5	80
8	17 500	14 000	0.00 (dry)	—	290
9	17 500	14 000	0.20–0.25	50.0–62.5	290

recorded, as well as the weight of the water after running the actuator. For the 80 s duration wet cases (2, 3, 5, and 7), the evaporation is approximated linearly using equation (1)

$$w_{\mathrm{w}} = (w_{\mathrm{i}} - w_{\mathrm{e}})\,\frac{t}{T} + w_{\mathrm{e}} \tag{1}$$

where w_{w} is the weight of the water subtracted from the total weight measured, w_{i} is the weight of water before the actuator is turned on, w_{e} is the weight of the water on the actuator after the actuator is turned off, t is the time elapsed since the beginning of the experiment, and T is the total time of experiment. This approximation is systemic and does not consider things such as steam evaporation and displacement of water due to ionic wind.

It is expected that the linear approximation will become inappropriate for a longer duration of time (say 290 s, case 8 and 9). This is because after a certain duration, water evaporation must decrease due to less water being available for evaporation. There are other important factors like temperature, vapor pressure, flow rate of air, humidity, amount of minerals dissolved in water that will also affect the evaporation rate. Hence, determining the rate of evaporation is quite complex and its accurate prediction is beyond the scope this work. It is generally expected that the evaporation rate will follow a logarithmic relation (e.g. Clausius–Clapeyron relation [36]). It is thus reasonable to approximate the weight of the water evaporated by the natural log as shown in equation (2).

$$w_{\mathrm{w}} = (w_{\mathrm{i}} - w_{\mathrm{e}})\ln(k \cdot t^{n} + 1) + w_{\mathrm{e}}. \tag{2}$$

Here the variables k and n are constants that determine the curve shape. The variable n is chosen to be 0.65 and k is calculated such that the weight of water evaporated, w_{w}, is at

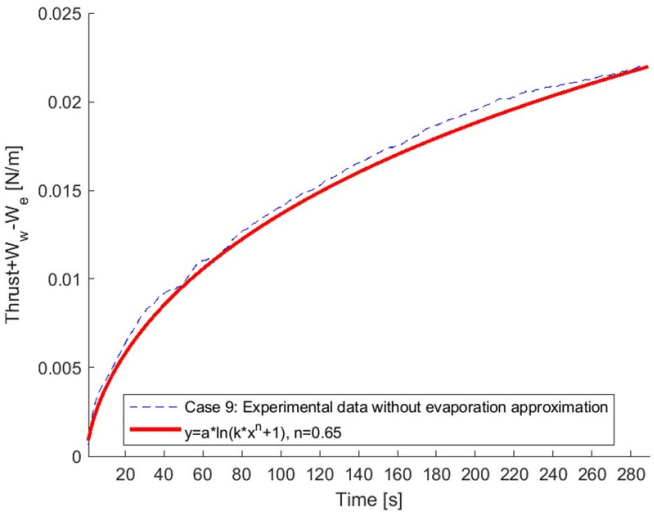

Figure 6. Curve fit for the thrust data without evaporation approximation. Here w_w is the weight of the water and w_e is the weight of water after running the actuator. The purpose of this fit is to find the appropriate value for n for the evaporation approximation in equation (2).

its max at the end of the run where $t = T$ assuming $w_e > 0$. The choice of $n = 0.65$ is because it is best fit for a function (y) which describes the weight measured by the scale without correction for water evaporated (see figure 6). This is under the assumption that most of the change in weight is due to water evaporation. Here a is the max weight measured.

3. Results and discussion

Actuators were run for 80 or 290 s for all cases shown in table 1. The 80 s cases were repeated five times while the 290 s cases were repeated three times. The high ambient RH (70%) present during actuator operation was expected to affect the thrust performance of the plasma actuators [28–30]. Note that the high RH not only reduces thrust but also reduces water evaporation rate. In general, plasma actuators follow $T \propto V^{\sigma}$ where T is the resultant thrust of a dry actuator, and V is the applied sinusoidal voltage. The parameter σ varies between 2 and 4 [4, 37, 38]. Wicks and Thomas found that thrust reduction followed a power law as a function of RH [30]. They found relative thrust reduction $(T - T_{dry})/T_{dry}$ is proportional to the ratio of vapor pressure P_v to saturation pressure P_{sat} as $(P_V/P_{sat})^{\beta}$. The power law exponent increases as RH is greater than 0.7, causing a large reduction in thrust and evaporation rate as RH approaches 1.

The average thrust and power data for each case are reported along with the error bar showing the spread of the data. In general, the measured thrust in dry actuator cases rises sharply for the first few seconds and then asymptotically approaches a quasi-steady value as time increases. This was also seen by Durscher and Roy [32]. Due to the simultaneous loss of energy in drying, the thrust of the wet actuator rises slowly with time, eventually approaching a lesser thrust magnitude as the actuator gradually becomes dry. The slow growth in thrust is most likely due to remnant water evaporating from the surface of the actuator, affecting the impedance of the system. Another factor which delays thrust recovery is the wicking of heat from the actuator surface. It is well known that once the plasma forms the actuator gradually heats up helping more electron production, and the thrust increases asymptotically to a steady state value [39]. When the water present on the actuator surface during plasma formation, some electrical energy is lost due to phase change evaporating the water delaying this asymptotic thrust increase.

From visual observation, as water droplets evaporate in some parts of the actuator, the plasma recovers unevenly, with visible glow forming arbitrarily depending on the drying pattern (See figure 13(c)). For the present set of experiments, the droplet size is quantified by identifying droplet shapes within two representative wet regions (one is a subset of the other, see figure 7) on the actuator surface by using *binarizing algorithm* using sensitivity threshold in MatLAB. The distribution of calculated nominal droplet diameters is plotted in figure 7. The smaller wet region in red is 20.5 × 18 mm in size. The bigger wet region in yellow 94.5 × 25 mm covers majority length of the exposed region of the actuator. Histogram for droplet diameter measured within these $L \times H$ sections of the actuator are shown below. Interestingly, the trendlines show a reasonable relation between number of droplets (N) and the droplet size D as $N = L \times H \times \exp(-15 \times D)$. The multidirectional lighting and perpendicular camera angle are fundamental to the binarization of the image with adaptive filtering in MatLAB. The droplets sufficiently distort the light enough to be darker than the plasma actuator surface. The resulting image is black and white with droplets in black. The *imfill* function is used to fill in the center of the droplets where light reflects as opposed to distorting. The droplet areas are measured using the *regionprops* function which measures the area in pixels, this is converted to millimeters. The mean radius is calculated from the area of a circle formula. The mean diameter for droplets is 0.35 mm, with the smallest droplets measured being 0.031 mm and largest being 4.8 mm.

In the test cases considered for this paper (see table 1), most droplets are between 0.03 and 0.5 mm in diameter. In comparison, diameter of a typical cloud droplet is 0.02 mm, and that of a typical raindrop is 2 mm [40]. It must be noted that when raindrops strike a stationary surface they may split into smaller droplets before they coalesce into a pool of water. In reality, rain may form a sub-mm thin layer of water on the surface of a moving vehicle. For these reasons, the nominal water droplet size of 0.03–0.5 mm studied in this paper may be considered of practical relevance.

Figure 8 plots the measured plasma induced thrust in Newtons per meter length of the electrode as a function of time for case 1, 2 and 3, with the actuator operating at 22.5 kV_{pp} and 14 kHz. The asymptotic peak thrust for the dry actuator after 80 s is about 20 mN m^{-1}. Although case 2 with 0.20–0.25 g of water and the case 3 with 0.50–0.60 g of water appear to nominally have the same mean thrust of about 15.8 mN m^{-1} (figure 6(a)) after 80 s, it can be seen from individual runs in figure 6(b) that case #3 with more water mass per unit surface

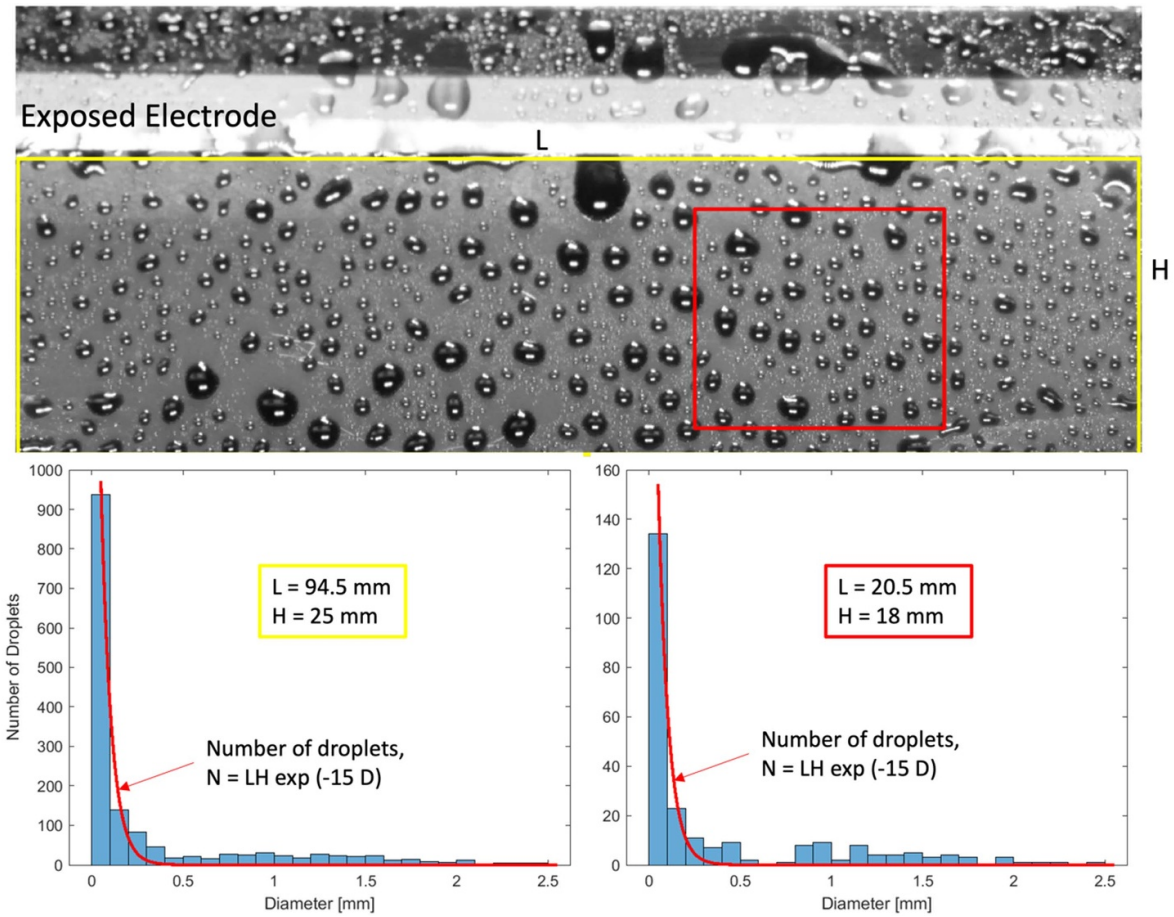

Figure 7. The photograph after applying ∼0.20–0.25 g of water to the actuator surface is shown on top with two regions of size $L \times H$ demarked. The bigger box in yellow is 94.5 × 25 mm in size and the smaller box in red is 20.5 × 18 mm in size. Histogram for droplet diameter measured within these $L \times H$ sections of the actuator are shown below. The trendlines show a reasonable relation between number of droplets (N) and the droplet size D in mm as $N = L \times H \times \exp(-15 \times D)$.

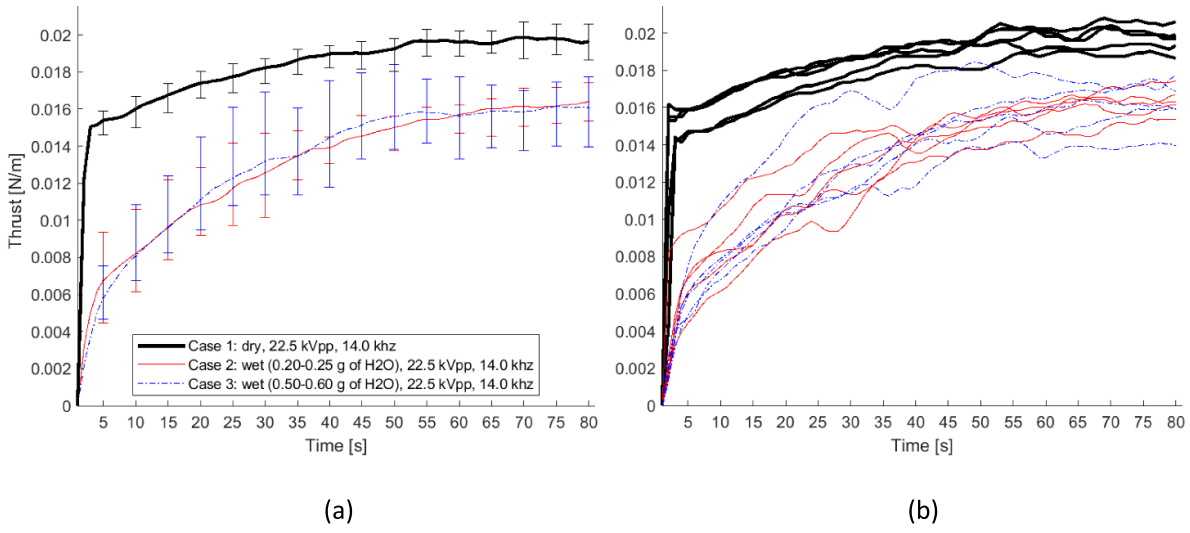

Figure 8. (a) Mean plots of case 1, case 2, and case 3. The error bars represent the minimum and maximum measured values from individual experiments shown in the right (b).

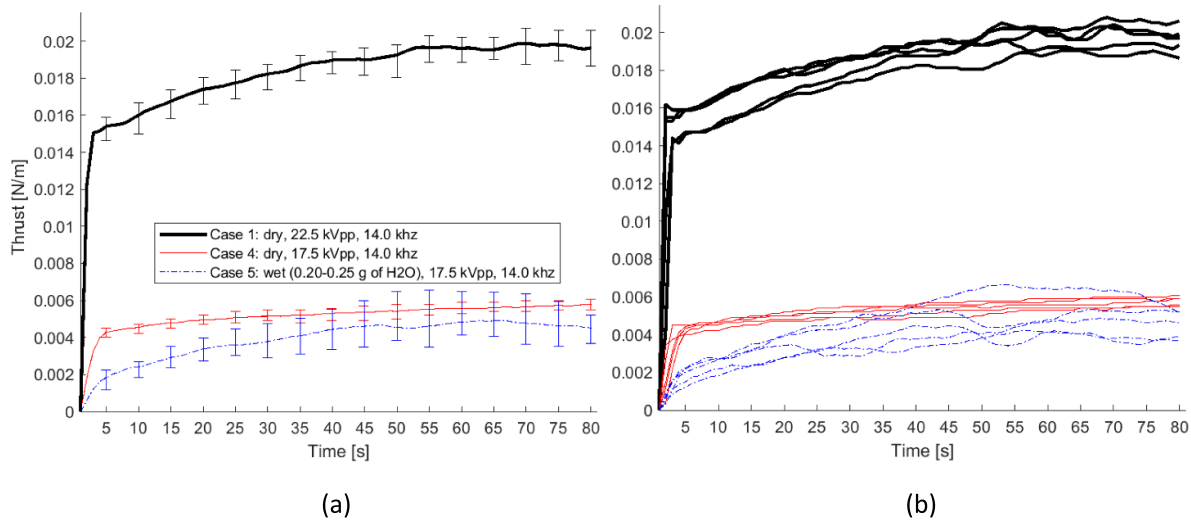

Figure 9. (a) Mean plots of case 1, case 4, and case 5. The error bars represent the minimum and maximum measured values from individual experiments shown in the right (b).

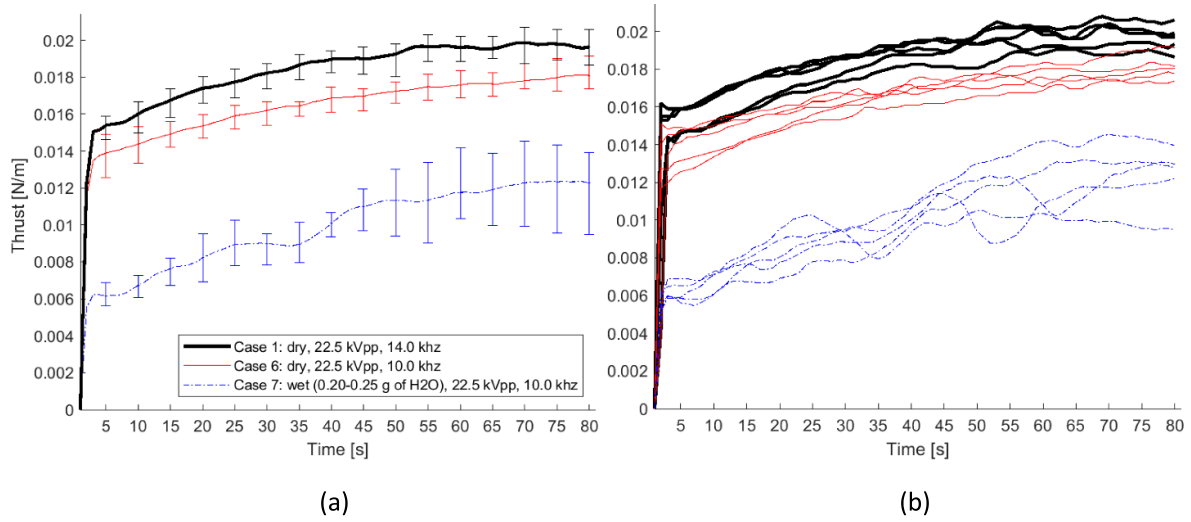

Figure 10. (a) Mean plots of case 1, case 6, and case 7. The error bars represent minimum and maximum measured values from individual experiments shown in the right (b).

area has more randomness in thrust recovery. This could be due to more accumulation water causing erratic formation of plasma, or due to the evaporation being very non-linear.

Figure 9 plots the lower voltage cases 4 and 5 operating at 17.5 kV_{pp} and 14 kHz. The measured thrusts in both cases were significantly less than case 1, 2 and 3 due to voltage difference. Interestingly, as time progresses the wet case 5 appears to recover thrust within the error margin of dry case 4, which measures about 5 mN m^{-1} at 60 s. This indicates that the actuator voltage has some effect on its ability to quickly recover from water deposition related performance delay. Lower operating voltage may take lesser recovery time for the same operating frequency.

The dry lower frequency case 6 operating at 22.5 kV_{pp} and 10 kHz is plotted in figure 10 that shows about 10% less measured thrust than its dry higher frequency counterpart (case 1) with 22.5 kV_{pp} and 14 kHz. The wet lower frequency case 7 operating at 22.5 kV_{pp} and 10 kHz, had significantly (∼30%) less thrust than its dry counterpart (case 6) even after 80 s. The data shows that a reduction in frequency may reduce a plasma actuator's rate of thrust recovery after direct water application. This is due to the fact that for a given voltage a reduction in frequency will result in a reduction in load power which in turn will reduce evaporation rate causing slower thrust recovery. Also important is to note that the measured thrust for the wet actuator operating at 10 kHz follows the rise curve of the dry actuator unlike the gradual thrust rise trend of the 14 kHz cases 2, 3 and 5.

To quantify the ability of a plasma actuator to recover from sprayed water, the ratio between the measured thrust for the wet case and the dry case (hereafter called the thrust ratio) is calculated at 5, 15, 25 and 80 s. When considering the results

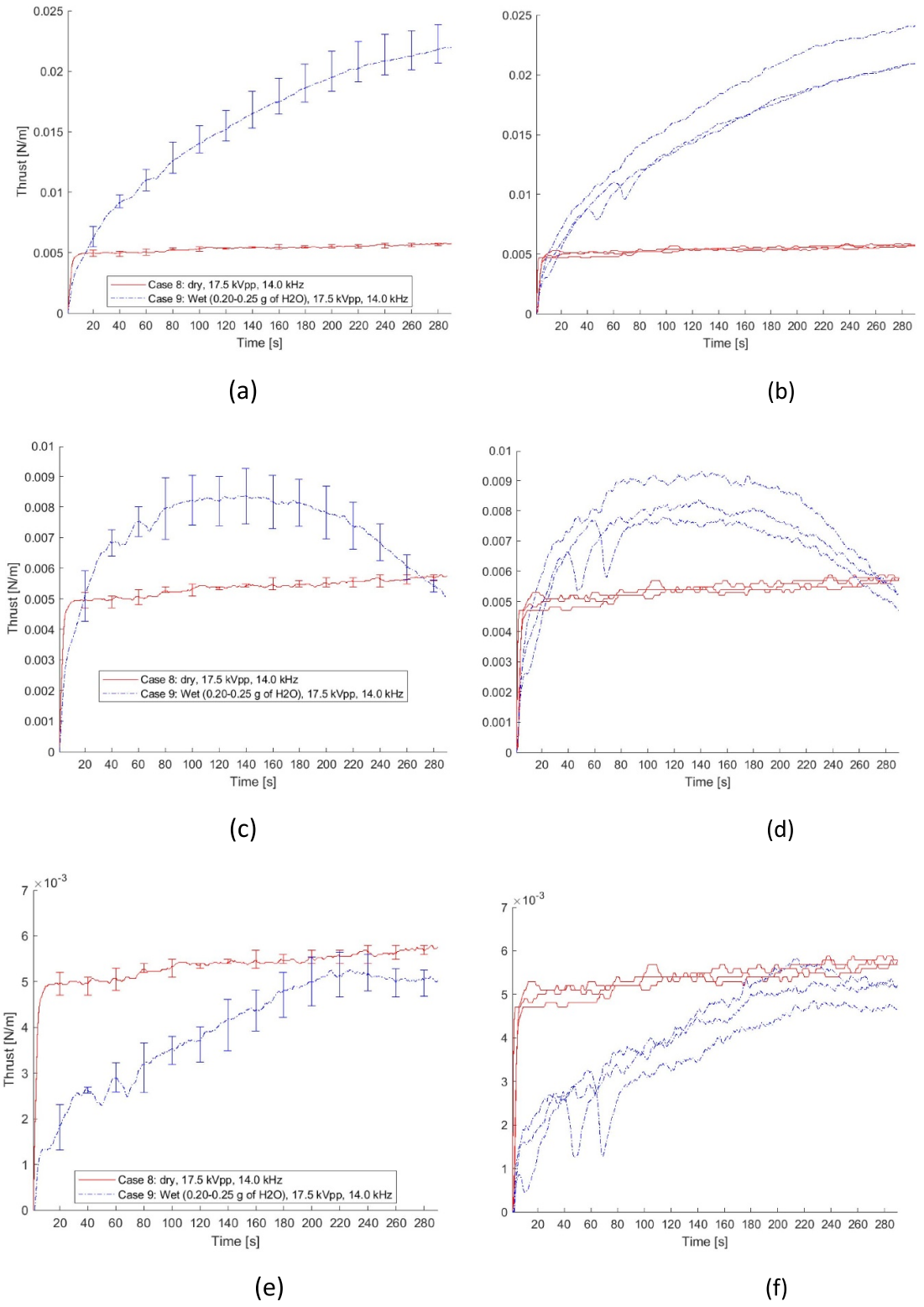

Figure 11. (a) Mean plot for case 8 and case 9 without any approximation for evaporation. (b) Raw data from individual experiments without any evaporation approximation. (c) Mean plot for case 8 and case 9 with a linear approximation for evaporation. (d) Individual experiments with linear evaporation approximation. (e) Mean plots of case 8 and case 9 for logarithmic evaporation approximation. The error bars represent minimum and maximum measured values from individual experiments shown in the right (f).

Table 2. Actuator thrust ratios.

Case	Thrust ratio at 5 s	Thrust ratio at 15 s	Thrust ratio at 25 s	Thrust ratio at 80 s
Case2 Case1	0.439	0.573	0.661	0.835
Case3 Case1	0.377	0.575	0.691	0.820
Case5 Case4	0.426	0.609	0.711	0.785
Case7 Case6	0.443	0.513	0.387	0.681

presented, it must be noted that saturated condition makes complete thrust recovery a particularly slow process compared to a dry or moderately humid actuator. Table 2 presents the thrust ratio for all cases. Noticeably the ratios vary in trend. Initially at 5 s, the thrust ratio for the low frequency case (case 7/case 6) is the highest but after 80 s the thrust ratio for the highest voltage and frequency case (case 2/case 1) dominates. At that time station thrust ratio for the lower frequency case (case 7/case 6) is significantly smaller than higher frequency cases. Interestingly, while the initial thrust ratio for higher water mass (case 3/case 1) is the lowest its recovery rate is also the fastest gaining back to the second highest thrust ratio of 0.820. The thrust ratio for the lower applied voltage case (case 5/case 4) is slightly lower than the highest voltage cases considered (case 2/case 1). This indicates that the time rate of recovery of the wet actuator may be slower at a lower voltage, but the rate (slope) considerably decreases with the decrease in applied frequency. Based on the experiments performed, it appears that the induced thrust of the wet actuator (T_w) is related to the applied frequency (f) as $T_w \propto f^{1.1}$. During testing it was observed that complete formation of plasma along the susceptible edge of the exposed electrode would only occur when the applied voltage is about 13 kV_{pp}. This is because air has a dielectric strength of 30 kV cm^{-1} and the actuators used for this study have dielectric thickness of 3 mm. Hence, cases 5 and 4 may suffer from weakest plasma formation for this actuator design.

To test the long-term recovery of the actuator two cases were observed, case 8 and case 9 (figure 11). These two cases were performed at 17.5 kV_{pp} and 14 kHz for 290 s. This time limit was chosen to avoid overheating of the amplifier. Case 8 was the dry case and case 9 was the case wetted with 0.20–0.25 g of water. The mean thrust of case 9 achieves over 90% thrust of case 8 indicating that a residual monolayer of water may be delaying the thrust recovery. It is anticipated that were the actuator run indefinitely, the thrusts for dry and wet cases would match. Considering that the water evaporation is approximated, it was decided to first compare between the direct measurement (no approximation) and a linear approximation for water evaporation.

The power consumption was calculated using the current at each time instance multiplied by the voltage then averaged over the entire time set and plotted in figure 12. This technique is the same as used by Durscher and Roy [32]. For every data point plotted an average of three readings each with 1 million measurement samples were taken. Each power measurement occurred over a period of 1 ms. As plotted in figure 12(a), the power consumption increased in case 2 with application of 0.20–0.25 g of sprayed water to the actuator. Incidentally, for the dry conditions (case 1), the power required after 5 s is 130 W m^{-1}. Corresponding wet case required 152 W m^{-1} power. After 25 s the wet actuator (case 2) consumed 172 W m^{-1} which is nearly 20% higher than the dry actuator (case 1). Figure 12(b) plots the ratio of plasma induced thrust over consumed power (thrust efficiency, aka thrust effectiveness) for the linear actuator under dry (case 1) and wet (case 2) conditions. Clearly the thrust generation per unit power consumed is significantly (>60%) lower for the wet conditions (case 2) than that for the dry conditions (case 1). Interestingly, the efficiency for the dry actuator stays relatively constant within the error band, while it rises almost linearly for the wet actuator during the 80 s testing period. The heating of the actuator appears to play some part in the extra consumption of power as the actuator dries beyond the region of plasma formation (see figure 13). The increased power consumption for the wet case causing lower efficiency may be due to an increase in the number of visible streamers (figure 13(c)) when operated with water adhesion. Over a long period of time, the streamers cause visible sputtering damage where they form near the exposed electrode as seen in figure 13(b). Other possible reasons for power consumption increase are current signature difference, ohmic heating of the water, dielectric tan loss of the actuator, higher impedance due to water, chemical interactions within the water, and plasma interaction with water vapor (dissociative and ionization related losses).

To further analyze the power data presented in figure 12, the current waveforms are plotted in figure 14. The rolling mean comparison of the discharge current (upper right) and its zoomed in peak A (lower right) shows the wet actuator has higher mean current even though the dry actuator has stronger ionization peaks. The rolling mean of any point i is calculated by taking the mean of $\pm m$ points around i which is chosen to be 300. This indicates that for wet actuator more power is lost in resistive heating.

Finally, as a general case of arbitrary actuator shape, figure 15 shows the transient evolution of the exposed surface after a continuously operating square serpentine actuator was completely wetted with water. Immediately after the water spray, the plasma glow quenches. However, as can be seen in figure 15(a), approximately after 1 s the purplish plasma

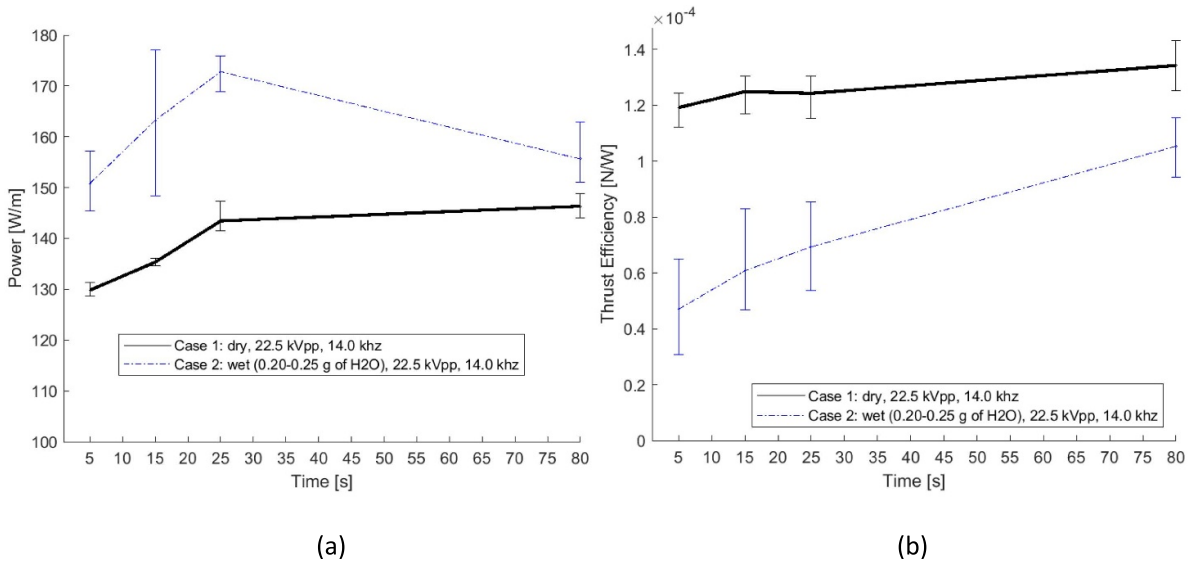

Figure 12. (a) The mean power consumption of the actuator for a dry (case 1) and a wet case (case 2) at 22.5 kV_{pp} and 14 kHz. (b) Thrust efficiency of the actuator. The error bars represent minimum and maximum measured values.

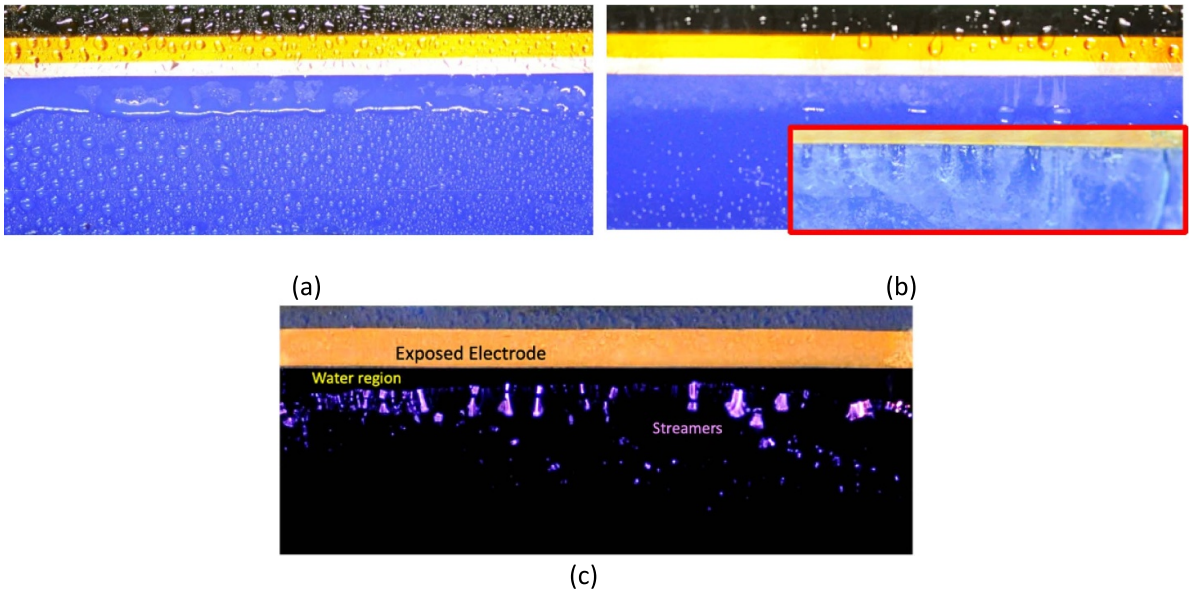

Figure 13. (a) A close-up picture of the plasma actuator before a 290 s run. (b) The surface after a 290 s run. In the red box inlay in (b) a close up of the damage near the exposed electrode is shown after approximately 10 h of continual operation. (c) Instantaneous image from a video of actuator operation with water droplets shows the streamers forming at the edge of water region.

glow reappears on the left side, and gradually fills up the entire near electrode region within about 5 s, figures 15(b)–(d), even though the water droplets are clearly visible just outside the plasma glow region. These experiments are run at 11.5 kV_{pp} and 8 kHz.

The mean power consumption data for the square serpentine actuator set are plotted in figure 16 and show similar trend to the linear actuator. The initial power consumption for the wet actuator is 62 w m^{-1} which is ∼61% higher than the dry actuator which remains reasonably steady at about 40 w m^{-1}. The wet actuator power requirement reduces with time as water droplets evaporate. At 80 s the wet case serpentine actuator consumes 40% more power than the dry serpentine actuator case. The slower power recovery may be due to the lower applied voltage and frequency, 11.5 kV_{pp} and 8 kHz, respectively.

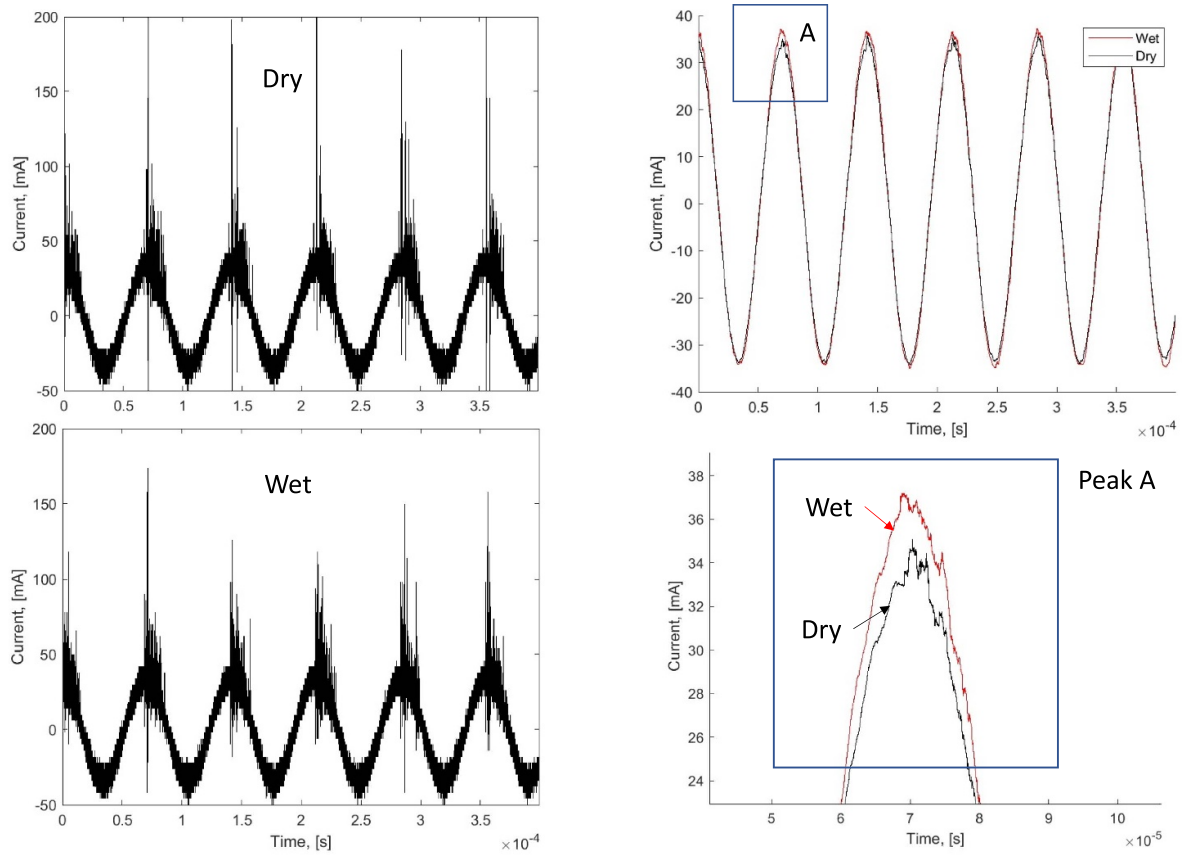

Figure 14. The current waveform under dry (upper left) and wet (lower left) conditions after 25 s show the difference in electrical performance between that the two conditions. The rolling mean comparison of the discharge current (upper right) and it is zoomed in peak (lower right) shows the wet actuator has higher mean current even though the dry actuator has stronger ionization peaks.

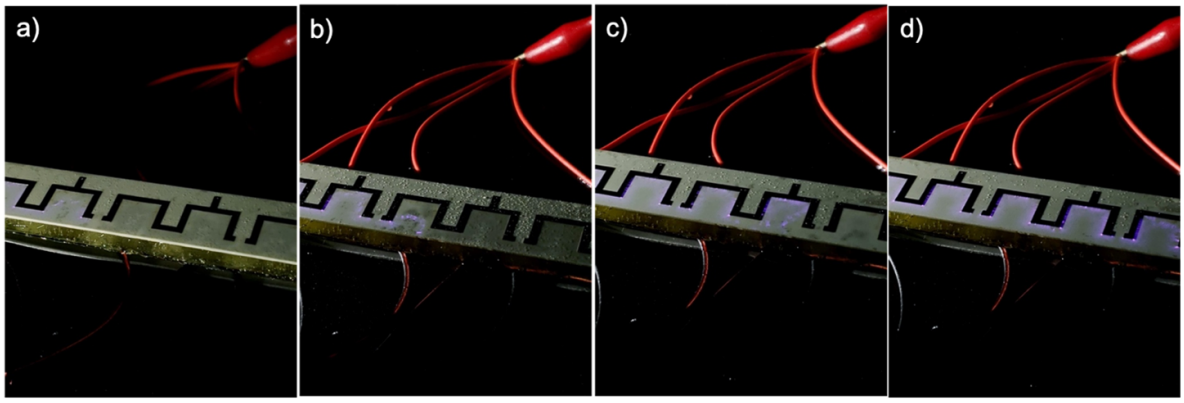

Figure 15. Images of a continuously operating serpentine shaped actuator after it was completely soaked with water spray showing transient recovery of plasma glow (a) ∼1 s, (b) ∼2 s, (c) ∼5 s, (d) ∼10 s.

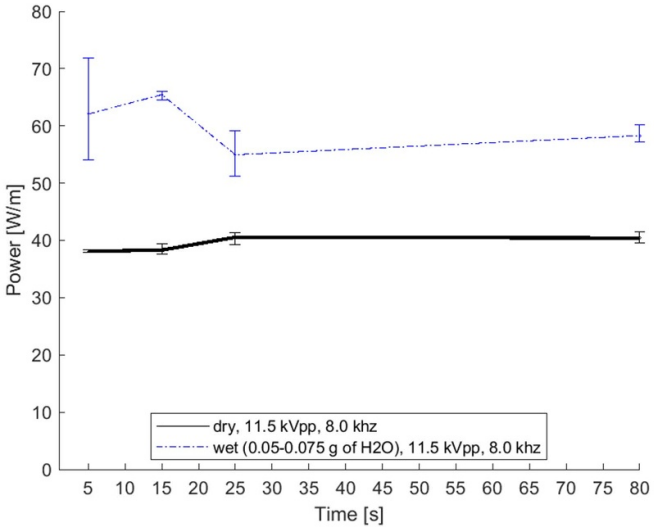

Figure 16. Power data for dry and wet tests of square serpentine actuator. The error bars represent minimum and maximum measured values.

4. Conclusion

The experiments performed seek to evaluate the performance of plasma actuators when they are subjected to direct water deposition on their surfaces. The experiments showed that linear plasma actuators can recover approximately 38% of the dry thrust within 5 s after water being applied to them. For the best case, 83.5% of the dry thrust was recovered within 80 s after water application. It appears that a decrease in voltage from 22.5 to 17.5 kV_{pp} at 14 kHz will marginally reduce a plasma actuator's ability to recover thrust (4% less thrust at 80 s compared to dry counterpart, table 2). By lowering the frequency from 14 to 10 kHz and maintaining a voltage of 22.5 kV_{pp}, the actuator recovered only 68.1% thrust of the dry case at 80 s (table 2). All cases except for the increased water application case (case 3) recovered by at least 42% of their dry thrust within 5 s. The increased water application case recovered 37.7% of its thrust. For cases run for 290 s (case 8 and 9), a near complete thrust recovery was achieved. Note the complete recovery may not have been achieved due to lingering presence of monolayer of water on the surface. As compared to its dry counterpart, power consumption in a wet actuator increases, lowering the thrust generation efficiency under wet condition. Comparison of discharge current plots show that while the dry actuator has higher ionization peaks the wet actuator rolling mean current is much higher indicating high impedance loss. This should be studied in future research to understand the cause of the electrical performance loss. The results of this study show that though authority of plasma actuators is negatively affected by direct water deposition, for engineering applications, they are still usably rugged even when completely wet, and can be effectively functional within a short timeframe. Note that the presence of an external flow constitutes an additional technical challenge requiring the implementation of complex test equipment which should be addressed in future experiments. The influence of water evaporation rate as functions of airflow, vapor pressure, on surface and in water contaminants should also be studied. The RH, temperature and external air velocity are very important control parameters for investigating the effects of water droplet adhesion. The evaporation at the moving plasma edge of the water droplets will generate a fluctuating nonuniform 3D thrust adding transient randomness which should be carefully studied. Future experiments should also compare the power data with Lissajous method for better confidence [41] in the electrical characterization of the wet system. The effect of additional thrust created by heated water molecules should also be carefully identified.

Data availability statement

All data that support the findings of this study are included within the article (and any supplementary files). Data is available from 01 October 2021.

Acknowledgments

The first author would like to acknowledge the Graduate Student Preeminence Award (GSPA) at the University of Florida and the Student Stem Employment Program (SSEP) under the United States Air Force for funding support and the AFRL contract OAI-C2644-19296. This work was also partially supported by a contract from NASA STTR Phase I 80NSSC19C0540 funded through SurfPlasma, Inc.

ORCID iD

Subrata Roy https://orcid.org/0000-0002-2316-0854

References

[1] Resler E L and Sears W 1958 The prospects for magneto-aerodynamics *J. Aerosp. Sci.* **25** 235–45
[2] Raizer Y P 1991 *Gas Discharge Physics* (Berlin: Springer)
[3] Roth J R 1995 *Industrial Plasma Engineering: Volume 1—Principles* (Bristol: Institute of Physics Publishing)
[4] Enloe C L, McLaughlin T E, VanDyken R D, Kachner K D, Jumper E J and Corke T C 2004 Mechanisms and responses of a single dielectric barrier plasma actuator: plasma morphology *AIAA J.* **42** 589–94
[5] Corke T, Enloe C L and Wilkinson S 2009 Dielectric barrier discharge plasma actuators for flow control *Annu. Rev. Fluid Mech.* **42** 505–29
[6] Wang J, Choi K, Feng L, Jukes T N and Whalley R D 2013 Recent developments in DBD plasmaflow control *Prog. Aerosp. Sci.* **62** 52–78
[7] Iranshahi K and Mani M 2018 Dielectric barrier discharge actuators employed as alternative to conventional high-lift devices *J. Aircr.* **55** 2104–13
[8] DasGupta A, Lilley A J, Dagen A A and Roy S Experimental study of serpentine plasma actuator for transition to turbulence *AIAA-2018-1553, SciTech 2018*
[9] DasGupta A and Roy S 2017 Three-dimensional plasma actuation for faster transition to turbulence *J. Phys. D: Appl. Phys.* **50** 425201

[10] Mullenix N J, Gaitonde D V and Visbal M R 2011 A plasma-actuator-based method to generate a supersonic turbulent boundary layer inflow condition for numerical simulations *AIAA Computational Fluids Dynamics, No. AIAA-2011* p 3556
[11] Roy S, Zhao P, Dasgupta A and Soni J 2016 Dielectric barrier discharge actuator for vehicle drag reduction at highway speeds *AIP Adv.* **6** 025322
[12] Lai C, Fu H, Hu B, Ling Z and Jiang L 2020 Aerodynamic Drag Reduction and Optimization of MIRA Model Based on Plasma Actuator *Actuators* **9** 64
[13] Kim D, Do H and Choi H 2020 Drag reduction on a three-dimensional model vehicle using a wire-to-plate DBD plasma actuator *Exp. Fluids* **61** 135
[14] Komuro A *et al* 2019 Influence of discharge energy on the lift and drag forces induced by a nanosecond-pulse-driven plasma actuator *Plasma Sources Sci. Technol.* **28** 065006
[15] Benard N, Jolibois J and Moreau E 2009 Lift and drag performances of an axisymmetric airfoil controlled by plasma actuator *J. Electrost.* **67** 133–9
[16] Kozlov A Z and Thomas F O 2011 Bluff-body flow control via two types of dielectric barrier *AIAA J.* **49** 1919–31
[17] Patel T K, Lilley A J, Shen W, Porrello C, Schindler-Tyka A, Roy S, Lear W E and Miller S A E 2021 Fundamental investigation using active plasma control to reduce blade–vortex interaction noise *Int. J. Aeroacoust.* **20** 870–900
[18] Keisar D, Hasin D and Greenblatt D 2019 Plasma actuator application on a full-scale aircraft tail *AIAA J.* **57** 616–27
[19] Gnemmi P, Charon R, Dupéroux J-P and George A 2008 Feasibility study for steering a supersonic projectile by a plasma actuator *AIAA J.* **46** 1308–17
[20] Cai J, Tian Y, Meng X, Han X, Zhang D and Hu H 2017 An experimental study of icing control using DBD plasma actuator *Exp. Fluids* **58** 102
[21] Liu Y, Kolbakir C, Hu H and Hu H 2018 A comparison study on the thermal effects in DBD plasma actuation and electrical heating for aircraft icing mitigation *Int. J. Heat Mass Transfer* **124** 319–30
[22] Chen Z 2020 A phenomenon study on spreading and evaporating process of droplet on DBD actuator for wind turbine anti-icing *IOP Conf. Ser.: Earth Environ. Sci.* **453** 012049
[23] Abe T, Takizawa Y and Sato S 2008 *AIAA J.* **46** 2248–56
[24] Benard N, Balcon N and Moreau E 2009 Electric wind produced by a surface dielectric barrier discharge operating in air at different pressures: aeronautical control insights *J. Phys. D: Appl. Phys.* **42** 042002
[25] Soni J and Roy S 2013 Low pressure characterization of dielectric barrier discharge actuators *Appl. Phys. Lett.* **102** 112908
[26] Wilkinson S P, Siochi E, Sauti G, Xu T, Meador M and Guo H 2014 Evaluation of dielectric-barrierdischarge actuator substrate materials *AIAA-2014-2810, 45th AIAA Plasmadynamics and Lasers Conf.* (*Atlanta, GA*) p 2810
[27] Portugal S, Roy S and Lin J 2017 Functional relationship between material property, applied frequency and ozone generation for surface dielectric barrier discharges in atmospheric air *Sci. Rep.* **7** 6388
[28] Anderson R and Roy S 2006 Preliminary experiments of barrier discharge plasma actuators using dry and humid air *AIAA-2006-0369, 44th AIAA Aerospace Sciences Meeting and Exhibit*
[29] Benard N, Balcon N and Moreau E 2009 Electric wind produced by a surface dielectric barrier discharge operating over a wide range of relative humidity *AIAA Aerospace Sciences Meeting, No. AIAA-2009-488*
[30] Wicks M and Thomas F O 2015 Effect of relative humidity on dielectric barrier discharge plasma actuator body force *AIAA J.* **53** 9
[31] Brandenburg R 2017 Dielectric barrier discharges: progress on plasma sources and on the understanding of regimes and single filaments *Plasma Sources Sci. Technol.* **26** 053001
[32] Durscher R and Roy S 2012 Evaluation of thrust measurement techniques for dielectric barrier discharge actuators *Exp. Fluids* **53** 1165–76
[33] Critical surface tension and contact angle with water for various polymers *Accu Dyne Test data* (available at: www.accudynetest.com/polytable_03.html?sortby=contact_angle)
[34] RO4000® Series High Frequency Circuit Materials Rogers Corporation (available at: www.mclpcb.com/wp-content/uploads/2021/05/Rogers-ro4000-laminates-ro4003c-and-ro4350b-data-sheet.pdf)
[35] Mylavarapu R 2004 Irrigation and household water test and interpretation: SL219/SS440, 10/2004 EDIS 2004 (https://doi.org/10.32473/edis-ss440-2004)
[36] Lawrence M G 2005 The relationship between relative humidity and the dewpoint temperature in moist air: a simple conversion and applications (PDF) *Bull. Am. Meteorol. Soc.* **86** 225–33
[37] Thomas F O, Corke T C, Iqbal M, Kozlov A and Schatzman D 2009 Optimization of dielectric barrier discharge plasma actuators for active aerodynamic flow control *AIAA J.* **47** 2169–78
[38] Singh K and Roy S 2008 Force approximation for a plasma actuator operating in atmospheric air *J. Appl. Phys.* **103** 013305
[39] Durscher R, Stanfield S and Roy S 2012 Characterization and manipulation of the "saturation" effect by changing the surface temperature of a dielectric barrier discharge actuator *Appl. Phys. Lett.* **101** 252902
[40] Sizes of Aerosols, Raindrop and Cloud Droplets UCAR Center for Science Education (available at: https://scied.ucar.edu/image/aerosols-raindrop-cloud-droplets-sizes)
[41] Ashpis D E, Laun M C and Griebeler E L 2017 Progress toward accurate measurement of dielectric barrier discharge plasma actuator power *AIAA J.* **55** 2254–68